Two-photon dissociation of the NO dimer in the region 7.1–8.2 eV: Excited states and photodissociation pathways

V. Dribinski, A. B. Potter, I. Fedorov, and H. Reisler

Citation: The Journal of Chemical Physics **121**, 12353 (2004); doi: 10.1063/1.1825381
View online: http://dx.doi.org/10.1063/1.1825381
View Table of Contents: http://scitation.aip.org/content/aip/journal/jcp/121/24?ver=pdfcov
Published by the AIP Publishing

Two-photon dissociation of the NO dimer in the region 7.1–8.2 eV: Excited states and photodissociation pathways

V. Dribinski, A. B. Potter, I. Fedorov, and H. Reisler
Department of Chemistry, University of Southern California, Los Angeles, California 90089-0482

(Received 8 September 2004; accepted 6 October 2004)

A study of excited states of the NO dimer is carried out at 7.1–8.2 eV excitation energies. Photoexcitation is achieved by two-photon absorption at 300–345 nm followed by $(NO)_2$ dissociation and detection of electronically excited products, mostly in $n=3$ Rydberg states of NO. Photoelectron imaging is used as a tool to identify product electronic states by using non-state-selective ionization. Photofragment ion imaging is used to characterize product translational energy and angular distributions. Evidence for production of NO($A\,^2\Sigma^+$), NO($C\,^2\Pi$), and NO($D\,^2\Sigma^+$) Rydberg states of NO, as well as the valence NO($B\,^2\Pi$) state, is obtained. On the basis of product translational energy and angular distributions, it is possible to characterize the excited state(s) accessed in this region, which must possess a significant Rydberg character. [DOI: 10.1063/1.1825381]

I. INTRODUCTION

Studies of highly excited electronic states of molecules present significant experimental and theoretical challenges. The increased density of electronic states leads to a high probability of intramolecular interactions and multiple decay channels—radiative, nonradiative, and dissociative. Experimental studies of highly excited states are hampered by technical difficulties as well as complexity of data interpretation, and are mostly limited to studies of resonance enhanced multiphoton ionization (REMPI). At the same time, the characterization of such states and their couplings to bound states and/or dissociative continua is essential for complete understanding of many atmospherically important photochemical processes, as well as the development of accurate quantum-mechanical models.

The nitric oxide dimer $(NO)_2$ has attracted considerable attention recently because of its unique bonding character that involves the singly-occupied antibonding orbitals of the NO monomers.[1–3] The resulting N–N bond is weak (710 ± 10 cm^{-1}) (Refs. 4–6) and its behavior is intermediate between van der Waals and covalent binding.[6,7] Its electronic structure and photodissociaton dynamics have intrigued both experimentalists and theorists. The low-lying electronic states of the dimer, which are located below 1 eV, correlate with two NO($X\,^2\Pi$) fragments,

$$(NO)_2 \rightarrow NO(X\,^2\Pi) + NO(X\,^2\Pi), \quad \Delta H = 710 \text{ cm}^{-1}(0.088 \text{ eV}). \tag{I}$$

Seven such excited states were predicted and investigated by *ab initio* methods,[1–3] but have yet to be observed experimentally. Experimental studies of electronically excited states have thus far focused on the near UV region (5.0–6.2 eV) where two additional dissociation channels have been observed and investigated[6–13]

$$(NO)_2 \rightarrow NO(A\,^2\Sigma^+) + NO(X\,^2\Pi), \quad \Delta H = 44\,910 \text{ cm}^{-1}(5.57 \text{ eV}) \tag{II}$$

$$(NO)_2 \rightarrow NO(B\,^2\Pi) + NO(X\,^2\Pi), \quad \Delta H = 46\,190 \text{ cm}^{-1}(5.73 \text{ eV}). \tag{III}$$

The origin of the lowest of these states was determined by photoelectron and photoion imaging studies to be at 5.12 eV. These studies, carried out at excitation energies below the dissociation threshold for channels (II) and (III), together with preliminary *ab initio* calculations, provide evidence for assigning the optically excited state as a mixed Rydberg $(3p)$/valence state.[14] It was suggested that strong absorption to this state is important up to at least 6.3 eV. The excited state, which is bound by at least 3500 cm^{-1}, is predissociative and products appear on a time scale of a few picoseconds.[6–13]

In the present paper we extend our studies of the photodissociation of the NO dimer to the region 7.1–8.2 eV, accessed by two-photon excitation at 300–345 nm. This excitation region contains a manifold of Rydberg and valence states but is below the energy where ion-pair states are predicted to lie.[1] By using photoelectron imaging, we identify channel (II) as a major pathway, and observe for the first time the two channels,

$$(NO)_2 \rightarrow NO(C\,^2\Pi) + NO(X\,^2\Pi), \quad \Delta H = 53\,081 \text{ cm}^{-1}(6.58 \text{ eV}) \tag{IV}$$

$$(NO)_2 \rightarrow NO(D\,^2\Sigma^+) + NO(X\,^2\Pi), \quad \Delta H = 54\,002 \text{ cm}^{-1}(6.70 \text{ eV}). \tag{V}$$

We also find evidence for the participation of channel (III). From analyses of photoelectron spectra of products, as well

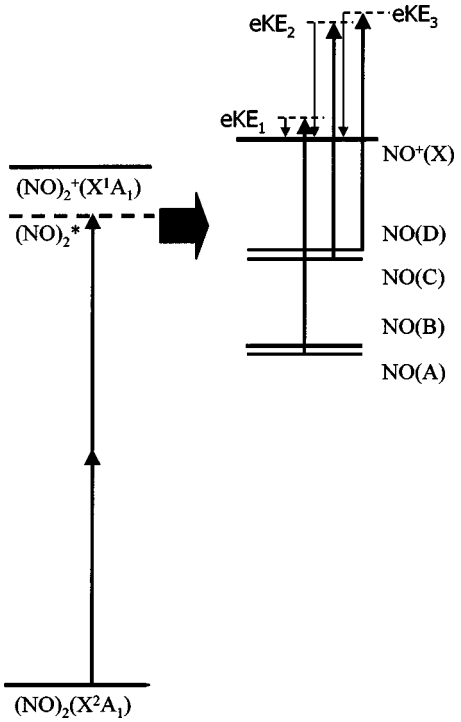

FIG. 1. Schematic diagram of two-photon excitation of $(NO)_2$ with subsequent detection of NO(A), NO(C), and NO(D) fragments by one-photon nonresonant ionization at the same photon energy via $\Delta v=0$ transitions.

as their translational and angular distributions (obtained by velocity map imaging), we are able to characterize the excited electronic state of the dimer accessed optically in this energy region. Most likely it has a significant Rydberg character, is weakly bound, and it predissociates via nonadiabatic couplings to lower Rydberg and valence states.

II. EXPERIMENTAL METHODS

The experimental arrangement has been described elsewhere,[14,15] and only relevant experimental details are presented here. Vibrationally and rotationally cold $(NO)_2$ molecules ($T_{\mathrm{rot}}=3-5$ K) are obtained in a molecular beam by supersonic expansion of gas mixtures containing 10%–20% NO in He at a backing pressure of 2 atm.[7] The NO dimer is promoted to 7.1–8.2 eV by two-photon transitions at 300–345 nm. The radiation is generated by frequency doubling the linearly polarized output of a Nd:YAG (YAG—yttrium aluminum garnet) laser pumped dye laser system (Spectra-Physics GCR230 with Continuum ND6000, Rhodamine 640, and DCM; 0.2–0.5 mJ; 40–50 cm focal-length lens, $\tau_{\mathrm{pulse}}=5-10$ ns). Following two-photon absorption, the NO dimer dissociates producing NO fragments in $3s$ and $3p$ Rydberg states [channels (II), (IV), and (V)]. These fragments are ionized *nonselectively* by one-photon absorption at the same wavelength, provided the photon energy exceeds the ionization energy of the Rydberg state via $\Delta v=v^{+}-v^{\mathrm{Ry}}=0$ transitions, where v^{+} and v^{Ry} are the vibrational levels of the ion and Rydberg states, respectively. The excitation scheme is shown in Fig. 1.

The velocity map imaging technique,[16,17] combined with event counting and centroiding[18,19] and the basis set expansion Abel (BASEX) transform method,[20] is used to obtain angular and translational energy distributions of either photoelectrons or NO^{+} ions.

In order to confirm that the measured signals originate from two-photon dissociation of the NO dimer followed by one-photon ionization of the products, the dependencies of these signals on NO concentration and laser energy are measured. Both photoelectron and NO^{+} ion signals exhibit identical dependencies on concentration and laser power with exponents of 1.6 ± 0.3 and 2.6 ± 0.4, respectively. The nearly quadratic NO concentration dependence confirms that the observed NO products derive from $(NO)_2$. The laser power dependence justifies the assumption that two-photon dissociation followed by partially saturated one-photon ionization of NO photofragments in Rydberg states leads to the observed photoelectrons and NO^{+} ions.

The only background signal observed in our experiments results from nonresonant three-photon ionization of cold NO in the molecular beam. However, this background constitutes less than 1% of the total signal in our experiments and can be ignored.

III. RESULTS AND DISCUSSION

A. Photoelectron kinetic energy distributions: Identification of dissociation channels

As stated above, several dissociation channels are energetically accessible in the region of study. At first glance it may seem impossible to distinguish among these channels in a one-color experiment. However, owing to the Rydberg nature of the $A\,^2\Sigma^+$, $C\,^2\Pi$, and $D\,^2\Sigma^+$ product states of NO, generated via channels (II), (IV), and (V), respectively, they can be unambiguously identified in the product photoelectron spectra. There are two major factors that make the assignments possible.

The geometries and electronic core structures of the $A\,^2\Sigma^+$, $C\,^2\Pi$, and $D\,^2\Sigma^+$ Rydberg states of NO are similar to those of the $NO^{+}(X\,^1\Sigma^+)$ ion, which results in similar rovibrational energy levels and a strong propensity for ionization via diagonal ($\Delta v=0$) transitions (the Franck–Condon factors for such transitions exceed 0.99).[21] As a consequence, ionization of different vibrational levels within the same Rydberg state produces photoelectrons with almost equal kinetic energies, and the photoelectron spectra consist of sets of well-resolved narrow peaks, each corresponding to ionization of a specific NO Rydberg state. In addition, ionization corresponding to the peak in the photoelectron kinetic energy (eKE) spectrum of each Rydberg state captures most of the Franck–Condon-active vibrational states of the ion and, therefore, the ionization probability is large. In contrast, ionization from the $X\,^2\Pi$ and $B\,^2\Pi$ valence states gives rise to a broad vibrational state distribution in the ion, and ionization at a specific wavelength may capture energetically only a subset of these states. Moreover, since the electronic configuration of $B\,^2\Pi$ requires excitation of an inner electron, two-electron excitation is needed to produce the ground $X\,^1\Sigma^+$ state of NO^{+}, leading to substantially lower probabilities for one-photon ionization.[22] Thus, the observed

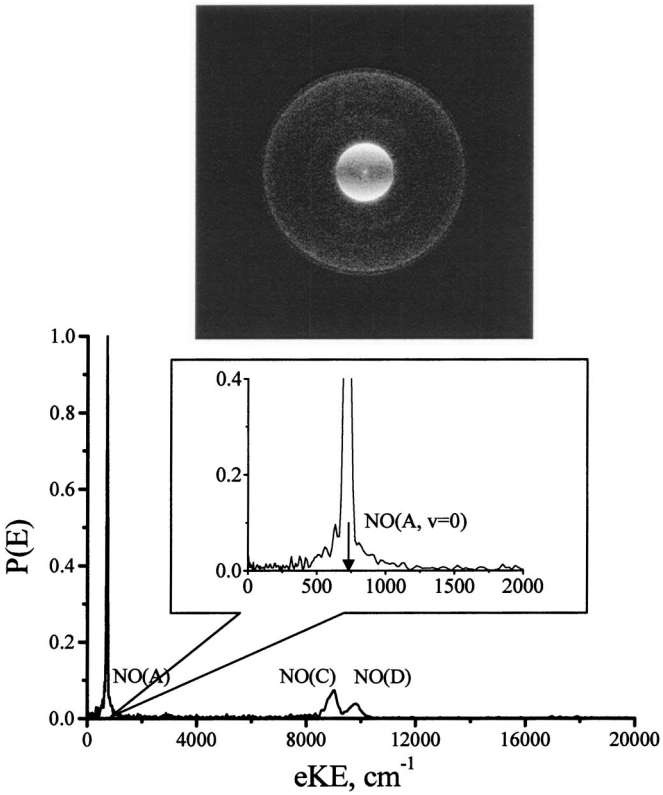

FIG. 2. Photoelectron image and the corresponding eKE obtained following two-photon excitation of $(NO)_2$ at 320 nm. The three peaks correspond to ionization of NO($A\,^2\Sigma^+$), NO($C\,^2\Pi$), and NO($D\,^2\Sigma^+$) produced in dissociation of the NO dimer. The inset shows the position and width of the NO($A\,^2\Sigma^+$) peak in more detail (see text).

product photoelectron spectrum reflects predominantly ionization of Rydberg states of NO.

Figure 2 shows a photoelectron image obtained from the ionization of NO fragments arising from two-photon dissociation of $(NO)_2$ at 320 nm ($2h\nu = 7.75$ eV) and the corresponding photoelectron translational energy distribution obtained by integrating the total intensity at each radius over all angles. Several conclusions can be drawn from this figure. First, three distinct narrow rings are observed in the image, corresponding to three narrow peaks in the eKE distribution. The positions of these peaks agree with those calculated for one-photon ionization of the $A\,^2\Sigma^+$, $C\,^2\Pi$, and $D\,^2\Sigma^+$ Rydberg states of NO (730, 8899, and 9820 cm^{-1}, respectively). Therefore, we conclude that reactions (2), (4), and (5) participate in 7.75 eV photodissociation.

Second, by integrating the area of each photoelectron peak, we obtain the relative yields of the three Rydberg states NO(A):NO(C):NO(D) = 1.00:0.48 ± 0.01:0.27 ± 0.02. This estimate is based on the assumption that the ionization probabilities for these states are comparable, as justified by the identical laser power dependencies for all three peaks. Note that production of NO(A) remains the dominant dissociation channel even though the excitation energy is 2.18 eV higher than the threshold of channel (II). Channels (IV) and (V), whose thresholds are higher, are also observed.

Third, analysis of the width of the low eKE peak [corresponding to ionization of NO(A)] shows that the full width at half maximum of this feature is 55 cm^{-1}. Such a narrow peak can only be a result of ionization of one or two vibrational levels in NO(A). However, levels NO($A, v = 0-7$) are accessible at 7.75 eV via channel (II). Due to the slight differences in spectroscopic constants for NO(A) and $NO^+(X)$,[23] photoelectrons resulting from ionization of NO($A, v = 7$) would have a kinetic energy of 1060 cm^{-1}, i.e., 330 cm^{-1} higher than that of photoelectrons generated by ionization of NO($A, v = 0$). The observed eKE peak position (maximum at 720 cm^{-1}) and the narrow width provide strong evidence for low vibrational excitation in the NO(A) fragment. No definitive conclusion about vibrational excitation of NO(C) and NO(D) fragments can be drawn from the photoelectron spectrum, because the measured relative widths of the peaks ($\Delta E/E = 4.7\%$ and 5.1% for C and D states, respectively) are close to the resolution limit of our imaging setup.

Photoelectron spectra exhibiting similar peaks corresponding to NO(A, C, D) products are obtained at other excitation energies up to 8.18 eV, and their ratios do not vary significantly with energy. Production of higher Rydberg states is not observed, even though the thresholds for NO($E\,^2\Sigma^+$) + NO($X\,^2\Pi$), NO($F\,^2\Delta$) + NO($X\,^2\Pi$), and NO($H\,^2\Sigma^+, H'\,^2\Pi$) + NO($X\,^2\Pi$) (7.63, 7.78, and 7.86 eV, respectively) are lower than the excitation energy. Minor traces of these states are detected in the photoelectron spectra at higher laser intensities, but these weak features exhibit much stronger laser power dependencies and are attributed to accidental 2+1 REMPI signals of either cold NO in the molecular beam or vibrationally/rotationally excited NO(X) fragments.

At wavelengths longer than 330.4 nm, none of the energetically allowed vibrational states of NO(A) can be ionized by one-photon absorption via $\Delta v = 0$ transitions, and the ionization probability of NO(A) becomes negligible compared to those of NO(C) and NO(D). Hence, channels (IV) and (V) can be studied selectively, which proves especially helpful in interpreting the NO^+ photofragment translational energy distributions (see below). A typical photoelectron image, obtained at $\lambda = 345$ nm ($2h\nu = 7.19$ eV), and the corresponding eKE distribution are depicted in Fig. 3. As expected, only two major features remain and they correspond to the ionization of NO(C) and NO(D) products with relative integrated peaks, NO(C):NO(D) = 1.00:0.39 ± 0.01. Again, the product ratios do not vary significantly in the 331–345 nm range.

The low-intensity features observed at lower kinetic energies are assigned as ionization of NO(B) products generated via channel (III). The assignment is based on the correspondence between spectral features and calculated photoelectron energies and Franck–Condon factors for one-photon ionization of the NO(B) state at 345 nm (see Fig. 3 and Appendix). The probability for direct one-photon ionization of NO(B) to $NO^+(X)$, though low, is non-negligible.[22] In some cases, such ionization can be facilitated by participation of highly excited neutral Rydberg states lying above the first ionization asymptote, followed by autoionization.[24] The integrated intensity of the NO(B) photoelectron signal at 345 nm is comparable to that of the NO(C) state. Taking

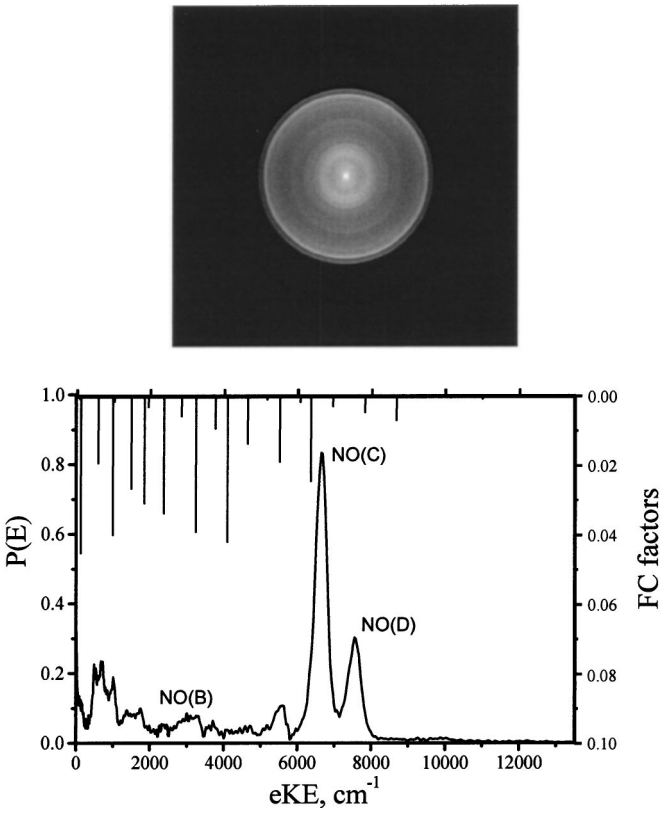

FIG. 3. Photoelectron image and the corresponding eKE obtained following two-photon excitation of $(NO)_2$ at 345 nm. The two large peaks correspond to ionization of NO($C\ ^2\Pi$) and NO($D\ ^2\Sigma^+$). The short vertical bars show the positions of possible ionization peaks of NO($B\ ^2\Pi$). The length of the line is proportional to the FC factor (right scale).

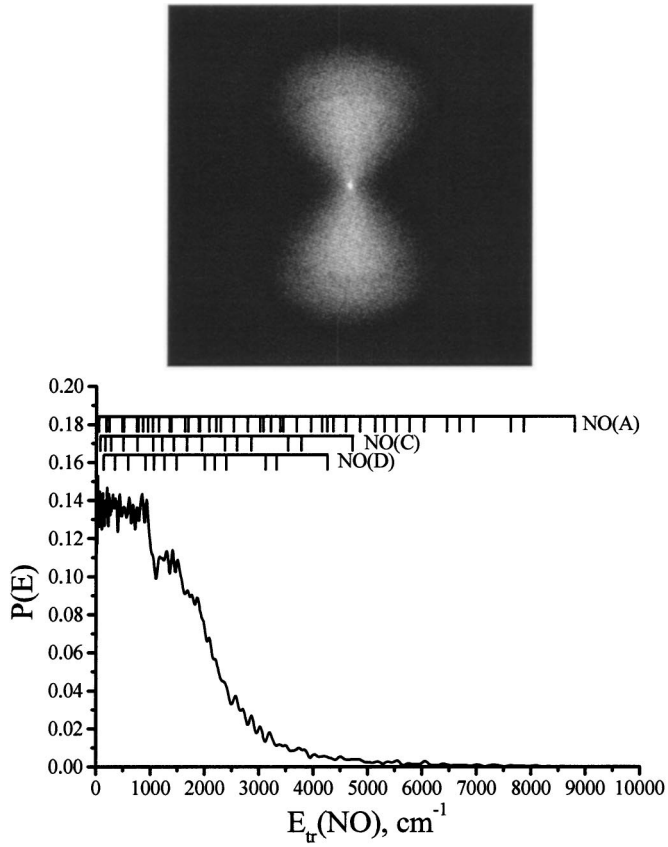

FIG. 4. Ion image and the corresponding translational energy distribution of NO^+ ions resulting from the ionization of products of two-photon dissociation of $(NO)_2$ at 320 nm. The short vertical bars in the upper part of the plot show the thresholds for the production of different vibrational states of ground and three Rydberg states of NO.

into account the low detection probability of the NO(B) state and the limited number of the vibrational levels that can be detected, we conclude that channel (III) is more populated than channels (IV) and (V). At 320 nm the contribution of NO(B) product to the photoelectron signal, though still detectable, is considerably smaller relative to products in A, C, and D states.

B. Photofragment translational energy distributions

While photoelectron spectra of dissociation products are used to identify product channels, ion translational energy distributions provide information on product internal excitations, and therefore on dissociation dynamics.

The image of NO^+ ions resulting from nonselective ionization of NO(A), NO(C), and NO(D) fragments generated in $(NO)_2$ dissociation at 320 nm is shown in Fig. 4, along with the corresponding ion translational energy distribution. No narrow features are resolved with this non-state-selective detection scheme. A large number of rotationally and vibrationally excited products are energetically allowed in the dissociation and, by energy conservation, this leads to a broad distribution of product kinetic energies (see marks in Fig. 4). However, one important conclusion can be drawn from the figure: the observed product translational energy distribution starts far below the maximum allowed energetically and peaks at low values. This indicates that the products are highly vibrationally and rotationally excited. Such conclusion is especially obvious for the NO(A)+NO(X) channel. At the same time, it was shown above that the NO(A) photoelectron spectrum at this wavelength is characteristic of a product that is rather cold vibrationally. Thus, we argue that most of the vibrational excitation is contained in the NO(X) cofragment.

Better resolved structures are seen in the 345 nm image (Fig. 5), where the NO(A) channel is not detected. The product translational energy distribution shown in Fig. 5 corresponds to very little vibrationally unexcited NO, and the most prominent feature can be assigned to NO($C,v=0$) +NO($X,v=2$) (see marks in the figure). Note that $v=2$ is the highest vibrationally excited level of NO(X) allowed by the energy available to channel (IV) at this excitation energy. In this regard, the dissociation dynamics is similar to that of the NO(A)+NO(X) channel.

Referring to Fig. 5, the observed distribution must also contain contributions from NO(B) produced via channel (III), as follows from the analysis of the corresponding photoelectron spectrum (Fig. 3). However, the photofragment translational energy distribution for this channel must be broad, because NO(B) in a range of vibrational states can be ionized. Consequently, this channel is expected to contribute little to the fragment signal at any given translational energy.

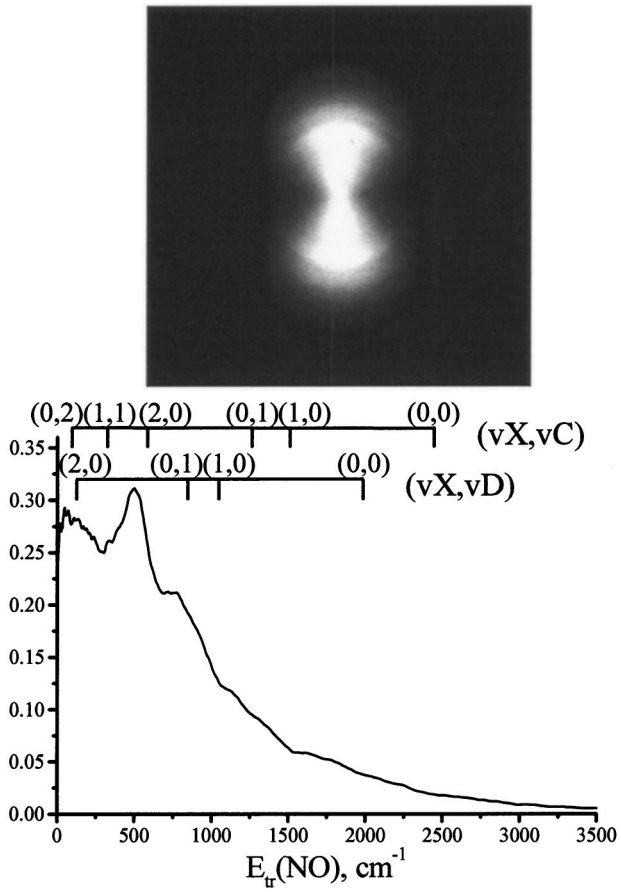

FIG. 5. Ion image and the corresponding translational energy distribution of NO^+ ions resulting from the ionization of the products of two-photon dissociation of the NO dimer at 345 nm. The thresholds for production of all the allowed vibrational states of NO($X\ ^2\Pi$), NO($C\ ^2\Pi$), and NO($D\ ^2\Sigma^+$) are shown with vertical bars.

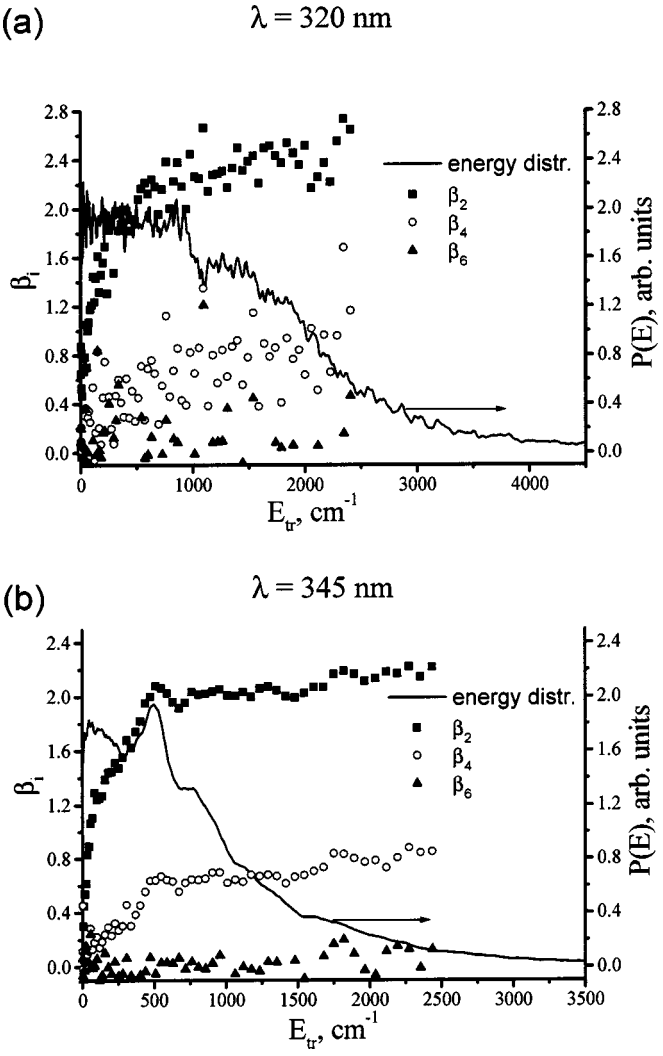

FIG. 6. Angular anisotropy parameters β_i obtained by fitting the experimental product angular distributions to Eq. (4). The corresponding translational energy distributions are shown for reference.

C. Photofragment recoil anisotropy

Due to the two-photon nature of the excitation step leading to dimer dissociation, the analysis of product angular distributions is more involved than in one-photon absorption of linearly polarized light followed by fast dissociation. In the latter case, the fragment angular distribution can be expressed by the well-known equation,[25]

$$I(\theta) = C[1 + \beta P_2(\cos\theta)], \tag{1}$$

where θ is the ejection angle with respect to the laser polarization axis, $P_2(x)$ is the second Legendre polynomial, C is the normalization constant, and β is the anisotropy parameter whose value is defined by the relative orientation of the fragment recoil direction with respect to the dipole moment of the initial transition. β is also sensitive to the dissociation lifetime and dynamics.[7,26,27]

The angular distributions of dissociation products in two-photon absorption can be obtained by multiplying distributions of the form of Eq. (1) for each of the two absorption steps and integrating over all possible intermediate steps (involving virtual and/or actual states of the parent molecule located at the energy of the first photon).[28] The equation becomes,

$$I(\theta) = C[1 + \beta_2 P_2(\cos\theta) + \beta_4 P_4(\cos\theta)], \tag{2}$$

where $P_4(x)$ is the fourth Legendre polynomial.

The meaning of the anisotropy parameters β_2 and β_4 can be understood by considering a few limiting cases. If the first photon absorption is dominated by only one intermediate state, then

$$I(\theta) = I_1(\theta) I_2(\theta), \tag{3}$$

where $I_1(\theta)$ and $I_2(\theta)$ are angular distributions of the form of Eq. (1) for the first and second photon absorptions, respectively. If both transitions are of parallel nature (i.e., the transition dipole moments lie parallel to the laser polarization axis) then $I_1(\theta) = I_2(\theta) \cong \cos^2\theta$ and $I(\theta) = C\cos^4\theta$, which corresponds to $\beta_2 = 20/7 \approx 2.86$ and $\beta_4 = 8/7 \approx 1.14$. In the case of one parallel and one perpendicular transitions, $I(\theta) = C\cos^2\theta\sin^2\theta$, $\beta_2 = 5/7 \approx 0.71$ and $\beta_4 = -12/7 \approx -1.71$; and for two perpendicular transitions $\beta_2 = -10/7 \approx -1.43$ and $\beta_4 = 3/7 \approx 0.43$.

The dependencies of the anisotropy parameters on product translational energies in two-photon dissociation of $(NO)_2$ at 320 and 345 nm are presented in Fig. 6. In order to confirm the two-photon nature of the dimer's excitation and

exclude the possibility of participation of higher-order excitations, the experimental angular distributions at each translational energy were fit with the extended equation,

$$I(\theta)=C[1+\beta_2 P_2(\cos\theta)+\beta_4 P_4(\cos\theta)+\beta_6 P_6(\cos\theta)], \quad (4)$$

which contains also a sixth Legendre polynomial responsible for three-photon processes. Figure 6 shows that at both wavelengths, β_2 and β_4 have nonzero values at all product translational energies, while $\beta_6 \approx 0$ within the accuracy of our experiments. It is also evident that at higher fragment translational energies both β_2 and β_4 have large positive values, producing a nearly $\cos^4\theta$ angular distribution. This indicates that a parallel transition with one dominating virtual intermediate state is accessed (no real dimer states are expected at the one-photon energy), and the transition dipole moments for both absorption steps are aligned along the N–N bond (i.e., B_2 symmetry in C_{2v} point group). Since the ground state of the NO dimer has A_1 symmetry, we conclude that the state (or states) initially accessed at 7.1–8.2 eV must also be of A_1 symmetry.

Both β_2 and β_4 decrease significantly in the region of low product translational energies (below 500 cm^{-1}). This trend has been observed previously for the anisotropy parameter β in one-photon dissociation of several molecules, including $(NO)_2$,[7,27,29] and successfully explained by a semiclassical model based on angular momentum conservation, which takes into account nonaxial recoil due to rotation of the molecular frame during dissociation of low-temperature species terminating in products with high rotational excitation. Likewise, the observed decrease in anisotropy parameters in our experiments indicates the formation of highly rotationally excited fragments.

The measured values of the anisotropy parameters at higher product translational energies are $\beta_2=2.5\pm0.1$, $\beta_4=0.9\pm0.1$ at 320 nm and $\beta_2=2.15\pm0.05$, $\beta_4=0.75\pm0.05$ at 345 nm. These values are close to the limiting values of $\beta_2=2.86$ and $\beta_4=1.14$ for a parallel transition with a parallel intermediate step. The slight reduction in the anisotropy parameters cannot be accounted for by the presence of a perpendicular component, because in this case one of the anisotropy parameters would have undergone a much larger reduction than the other (as demonstrated above, in perpendicular transitions β_2 and β_4 have opposite signs). The deviations from the maximum values of the anisotropy parameters at high product translational energies can be explained by rotation of the parent dimer prior to dissociation. Following the simple classical derivation of Jonah for one-photon transition,[30] we obtain for the case of two-photon dissociation,

$$\beta_2^{\mathrm{eff}}=\frac{\tau^2\omega^2+1}{4\tau^2\omega^2+1}\beta_2, \quad (5)$$

$$\beta_4^{\mathrm{eff}}=\frac{(\tau^2\omega^2+1)(9\tau^2\omega^2+1)}{(4\tau^2\omega^2+1)(16\tau^2\omega^2+1)}\beta_4, \quad (6)$$

where β_i $(i=2,4)$ is the anisotropy parameter for the nonrotating parent molecule, ω is its classical rotational angular velocity, and τ is a characteristic lifetime of the molecule before dissociation. Using Eqs. (5) and (6) with the experimental β_2 and β_4 values and a rotational temperature $T=3-5$ K for parent $(NO)_2$ in the beam, we obtain dissociation lifetimes of $\approx$0.7 ps and $\approx$1.2 ps at 7.75 eV (320 nm), and 7.19 eV (345 nm), respectively; i.e., the dissociation lifetime decreases at higher excitation energies. These lifetimes are longer than a vibrational period, implying a predissociative mechanism rather than direct dissociation from a repulsive excited state. Another indication of the predissociative nature of the excited state is the detection of a weak dimer-ion signal $(m/e=60)$ in excitation wavelengths in the region 7.1–8.2 eV. In other words, even with a nanosecond laser, ionization of the excited dimer state competes with dissociation. A predissociation mechanism can also explain the observed high internal (vibrational and rotational) excitation of the dissociation products.

D. The nature of the excited state

The experimental results described above allow us to characterize the optically excited state. The large signals from NO products in Rydberg states point to a correlation between the product channels and parent dimer excited state(s) with significant Rydberg character. The bound nature of the state is supported by the observation of a $(NO)_2^+$ parent ion signal in ionization via the neutral dimer's excited state. The $(NO)_2^+$ ion is bound by $\sim$5000 cm^{-1}, and the 5.12 eV excited state is bound by at least 3500 cm^{-1}. The observation of a dimer ion mass at $m/e=60$ confirms that the excited state of the neutral dimer has a lifetime long enough to allow ionization by a nanosecond laser beam. An absorption spectrum in this wavelength region is unavailable, but the 2+1 REMPI spectrum of the NO dimer at 300–345 nm appears to have diffuse structures.

Based on the A_1 symmetry of the excited state of the dimer and the energies of the dimer Rydberg states estimated by using the Rydberg formula,[31] four possible candidates emerge: $3d_{x^2}$, $3d_{x^2-y^2}$, $4s$ (estimated energies $\sim$7.2 eV), and $4p_z$ ($\sim$7.5 eV), where z is perpendicular to the N–N bond in the plane of the molecule (C_2 axis). The observed NO Rydberg products are all in $n=3$ states, and therefore correlate with $n=3$ Rydberg states of the dimer, providing some preference for the $3d$ states. However, experiments and calculations at lower energies show that a state with a specific Rydberg character in the dimer does not necessarily evolve adiabatically to product NO monomer in the corresponding Rydberg state.[14] The electronic state reached at 5.6 eV has a mixed B_2 valence/Rydberg $(3p_x)$ character, but the major product is NO in the $3s$ Rydberg state. In the present experiments the simultaneous production of several electronically excited states of NO indicates that more than one excited state of the NO dimer participates in the dissociation. This underscores the importance of nonadiabatic interactions between excited states in the region of study. Valence dimer states leading to NO products in excited valence states [e.g., NO(B)] probably participate as well, and states with a mixed valence/Rydberg nature are likely.

TABLE I. Calculated Franck–Condon factors for the ionization of NO($B\,^2\Pi, v=1-12$).

$v^B\,v^+$	0	1	2	3	4
1	$<4\times10^{-6}$	⋯	⋯	⋯	⋯
2	$<4\times10^{-6}$	⋯	⋯	⋯	⋯
3	$<4\times10^{-6}$	9.02×10^{-6}	⋯	⋯	⋯
4	$<4\times10^{-6}$	3.16×10^{-5}	⋯	⋯	⋯
5	4.51×10^{-6}	8.57×10^{-5}	7.26×10^{-4}	⋯	⋯
6	1.35×10^{-5}	2.16×10^{-4}	1.63×10^{-3}	⋯	⋯
7	3.15×10^{-5}	4.83×10^{-4}	3.22×10^{-3}	⋯	⋯
8	7.22×10^{-5}	9.65×10^{-4}	5.72×10^{-3}	1.93×10^{-2}	⋯
9	1.49×10^{-4}	1.77×10^{-3}	9.23×10^{-3}	2.68×10^{-2}	⋯
10	2.75×10^{-4}	2.98×10^{-3}	1.37×10^{-2}	3.38×10^{-2}	4.51×10^{-2}
11	4.83×10^{-4}	4.70×10^{-3}	1.89×10^{-2}	3.91×10^{-2}	3.99×10^{-2}
12	8.07×10^{-4}	7.00×10^{-3}	2.45×10^{-2}	4.18×10^{-2}	3.09×10^{-2}

IV. SUMMARY

Excited states of the $(NO)_2$ dimer in the 7.1–8.2 eV region were studied by two-photon dissociation and detection of NO^+ ions and photoelectrons produced by nonresonant ionization of excited NO products. Three Rydberg states of NO were identified as dissociation products: NO($A\,^2\Sigma^+$), NO($C\,^2\Pi$), and NO($D\,^2\Sigma^+$), all belonging to the $n=3$ Rydberg series. Evidence for production of NO($B\,^2\Pi$) is obtained as well. The NO($X\,^2\Pi$) fragments possess significant vibrational excitation, whereas the Rydberg NO cofragments are vibrationally colder. The products have large amounts of rotational excitation.

The time scale for dissociation is ~1 ps, typical of predissociation rather than direct dissociation from a repulsive state. The appearance of $(NO)_2^+$ parent ions in the REMPI spectrum confirms the bound nature of the optically accessible state. Based on the observed A_1 symmetry of the upper state and the Rydberg nature of the products, the initially excited dimer state may possess a significant $3d_{x^2}$, $3d_{x^2-y^2}$, $4s$, or $4p_z$ Rydberg character. Nonadiabatic transitions to other Rydberg and valence states lead to the final product channels.

This study demonstrates that photoelectron spectroscopy of products can serve as a useful tool in identifying product electronic states even in non-state-selective ionization.

ACKNOWLEDGMENTS

Support by the National Science Foundation and the Donors of the Petroleum Research Fund administered by the American Chemical Society is gratefully acknowledged. The authors thank Albert Stolow, Carl Hayden, Anna Krylov, and Sergei Levchenko for helpful discussions and sharing with them unpublished experimental and theoretical results.

APPENDIX: ONE PHOTON IONIZATION OF THE NO($B^2\Pi$) STATE AT 345 nm

NO($B\,^2\Pi$) fragments in $v=0-12$ are energetically allowed in the two-photon dissociation of the NO dimer at 345 nm via the NO($B\,^2\Pi$)+NO($X\,^2\Pi$) channel. NO(B) in $v=1-12$ can be ionized by one-photon absorption at the same wavelength, generating $NO^+(X\,^1\Sigma^+, v=0-4)$.

Photofragment fluorescence spectra obtained by Kajimoto *et al.* following one-photon dissociation of $(NO)_2$ at 193 nm revealed the presence of this channel with a broad vibrational distribution of the NO($B\,^2\Pi$) product that encompassed all the energetically allowed levels.[8] Therefore, we calculated Franck-Condon factors for transitions originating in $v=1-12$. Because the geometries of NO(B) and ground-state NO^+ are different,[23] all five accessible vibrational levels of the NO^+ ion are included.

In order to compute the Franck–Condon factors, vibrational eigenfunctions of both NO($B\,^2\Pi, v=0-12$) and $NO^+(X\,^1\Pi^+, v=0-4)$, as well as their overlaps, are calculated by using the Morse function[32] to model diatomic internuclear potentials. This is done with a computer program given in Ref. 33. Spectroscopic constants of NO(B) and $NO^+(X)$ are used to estimate the parameters of the Morse potential.[23] This approach results in a somewhat increased depth of the potential well in the NO(B) state (by ≈20%), but generates the correct positions of the vibrational energy levels. Therefore, this is a valid model for levels far below the dissociation asymptote of NO(B). However, we have also confirmed that the use of the experimental dissociation energy in the NO(B) Morse potential produces qualitatively similar Franck–Condon factors and, therefore, does not affect our conclusions.

The values of the Franck–Condon factors are summarized in Table I and also shown in Fig. 3 in the text.

As seen from the table, only higher ($v=8-12$) vibrational levels of the B state possess non-negligible Franck–Condon factors with the allowed ion states, and the positions of those transitions in the photoelectron spectrum are in good agreement with the observed low-intensity features (Fig. 3).

[1] A. L. L. East, J. Chem. Phys. **109**, 2185 (1998).
[2] R. Sayos, R. Valero, J. M. Anglada, and M. Gonzalez, J. Chem. Phys. **112**, 6608 (2000).
[3] M. Tobita, S. A. Perera, M. Musial, and R. J. Bartlett, J. Chem. Phys. **119**, 10713 (2003).
[4] J. R. Hetzler, M. P. Casassa, and D. S. King, J. Phys. Chem. **95**, 8086 (1991).
[5] E. A. Wade, J. I. Cline, K. T. Lorenz, C. Hayden, and D. W. Chandler, J. Chem. Phys. **116**, 4755 (2002).
[6] A. B. Potter, V. Dribinski, A. V. Demyanenko, and H. Reisler, J. Chem. Phys. **119**, 7197 (2003).
[7] A. V. Demyanenko, A. B. Potter, V. Dribinski, and H. Reisler, J. Chem. Phys. **117**, 2568 (2002).

[8] O. Kajimoto, K. Honma, and T. Kobayashi, J. Phys. Chem. **89**, 2725 (1985).
[9] Y. Naitoh, Y. Fujimura, O. Kajimoto, and K. Honma, Chem. Phys. Lett. **190**, 135 (1992).
[10] Y. Naitoh, Y. Fujimura, K. Honma, and O. Kajimoto, Chem. Phys. Lett. **205**, 423 (1993).
[11] Y. Naitoh, Y. Fujimura, F. Honma, and O. Kajimoto, J. Phys. Chem. **99**, 13652 (1995).
[12] V. Blanchet and A. Stolow, J. Chem. Phys. **108**, 4371 (1998).
[13] M. Tsubouchi, C. A. de Lange, and T. Suzuki, J. Chem. Phys. **119**, 11728 (2003).
[14] V. Dribinski, A. B. Potter, I. Fedorov, and H. Reisler, Chem. Phys. Lett. **385**, 233 (2004).
[15] A. Sanov, T. Droz-Georget, M. Zyrianov, and H. Reisler, J. Chem. Phys. **106**, 7013 (1997).
[16] A. Eppink and D. H. Parker, Rev. Sci. Instrum. **68**, 3477 (1997).
[17] E. Wrede, S. Laubach, S. Schulenburg, A. Brown, E. R. Wouters, A. J. Orr-Ewing, and M. N. R. Ashfold, J. Chem. Phys. **114**, 2629 (2001).
[18] B.-Y. Chang, R. C. Hoetzlein, J. A. Mueller, J. D. Geiser, and P. L. Houston, Rev. Sci. Instrum. **69**, 1665 (1998).
[19] Y. Tanaka, M. Kawasaki, Y. Matsumi, H. Fujiwara, T. Ishiwata, L. J. Rogers, R. N. Dixon, and M. N. R. Ashfold, J. Chem. Phys. **109**, 1315 (1998).
[20] V. Dribinski, A. Ossadtchi, V. A. Mandelshtam, and H. Reisler, Rev. Sci. Instrum. **73**, 2634 (2002).
[21] J. C. Miller and R. N. Compton, J. Chem. Phys. **75**, 22 (1981).
[22] H. Zacharias, F. de Rougemont, T. F. Heinz, and M. M. T. Loy, J. Chem. Phys. **105**, 111 (1996).
[23] *NIST Chemistry WebBook*, NIST Standard Reference Database No. 69, edited by P. J. Linstrom and W. G. Mallard (National Institute of Standards and Technology, Gaithersberg, 2003); http://webbook.nist.gov/chemistry/
[24] Y. Achiba, K. Sato, and K. Kimura, J. Chem. Phys. **82**, 3959 (1985).
[25] R. N. Zare and D. R. Herschbach, Proc. IEEE **51**, 173 (1963).
[26] H.-P. Loock, J. Cao, and C. X. W. Qian, Chem. Phys. Lett. **206**, 422 (1993).
[27] A. V. Demyanenko, V. Dribinski, H. Reisler, H. Meyer, and C. X. W. Qian, J. Chem. Phys. **111**, 7383 (1999).
[28] R. N. Zare, Mol. Photochem. **4**, 1 (1972).
[29] D. H. Mordaunt, M. N. R. Ashfold, and R. N. Dixon, J. Chem. Phys. **104**, 6460 (1996).
[30] C. Jonah, J. Chem. Phys. **55**, 1915 (1971).
[31] M. B. Robin, *Higher Excited States of Polyatomic Molecules* (Academic, New York, 1974).
[32] P. M. Morse, Phys. Rev. **34**, 57 (1929).
[33] D. W. Arnold, Ph.D. thesis, University of California, Berkeley, 1994.